Eur. Phys. J. D **27**, 239–246 (2003)
DOI: 10.1140/epjd/e2003-00281-7

THE EUROPEAN PHYSICAL JOURNAL D

Time-dependent 3-D modelling of laser surface heating for the hardening of metallic materials

V. Colombo[1,a], A. Mentrelli[1,b], and T. Trombetti[2,c]

[1] Dipartimento di Ingegneria delle Costruzioni Meccaniche, Nucleari, Aeronautiche e di Metallurgia (DIEM) and Centro Interdipartimentale di Ricerca per le Applicazioni della Matematica (CIRAM), Università degli Studi di Bologna, Via Saragozza 8, 40123 Bologna, Italy
[2] Dipartimento di Ingegneria delle Costruzioni Meccaniche, Nucleari, Aeronautiche e di Metallurgia (DIEM), Università degli Studi di Bologna, Viale del Risorgimento 2, 40136 Bologna, Italy

Received 29 July 2003
Published online 30 September 2003 –

Abstract. A numerical code for the time-dependent three-dimensional modelling of the laser surface heating for the hardening of metallic materials has been developed by the authors. The temperature-dependence of the thermal properties of the material (stainless steel) is taken into account in the frame of a heating process that doesn't lead to material melting or evaporation. Calculations have been carried out for various dimensions of the parallelepiped-shaped and of the square-shaped spot of the laser beam, as well as for different scanning velocity and for different levels of the laser source power. Various patterns of the laser spot path have also been studied, including a single-pass hardening pattern, a double-pass hardening pattern with and without overlapping, multiple discontinuous and continuous hardening patterns and spiral hardening patterns. The presented results show how the proposed model can be usefully employed in the prediction of the time-evolution of temperature distribution which arises in the workpiece as a consequence of the laser-workpiece interaction under operating conditions typically encountered in industrial applications of the laser hardening process.

PACS. 42.62.Cf Industrial applications – 44.05.+e Analytical and numerical techniques

1 Introduction

High-power laser facilities are widely used in industrial processes of welding, cutting, drilling as well as for surface treatments of materials. In particular, laser sources can provide a controllable high-density energy deposition in selected areas for producing thin hardened surface layers in a workpiece of metallic material (laser surface hardening, LSH). When a laser beam impinges on the surface of a workpiece, part of its energy is absorbed by the surface and suddenly turns into thermal energy. If this absorbed energy is high enough, heat is generated in this region at a rate higher than the rate at which it flows to the bulk of the material by conduction. In this circumstances, the temperature of the surface layers increases very quickly and in this region austenitization may occur, being the bulk temperature of the material essentially unaffected. Moving the workpiece with respect to the laser source, a point on the surface of the workpiece within the beam track is rapidly heated as the laser spot approaches it and passes, and is rapidly cooled by heat conduction to the bulk of the material after the beam has passed. By properly selecting the process parameters (power of the laser beam, relative laser source-workpiece velocity (scanning velocity), shape and dimensions of the workpiece area on which the laser beam impinges (laser spot), power distribution in the cross-section of the beam), the heating and cooling of the metallic material may be suitably controlled in order to allow hard martensite to form at the surface as a consequence of the treatment [1].

A lot of factors, besides the just mentioned process parameters, influence the evolution of the temperature distribution in the three-dimensional workpiece as a consequence of the laser-material interaction including the absorption coefficient of the workpiece, the properties of the treated material (such as its thermal conductivity, specific heat and emissivity) and the shape and dimensions of the workpiece itself [1,2]. When all these parameters are known, the thermal behaviour of the treated workpiece may be evaluated by means of analytical expressions available in the literature [1,3–10]. Yet, these expressions,

[a] e-mail: colombo@ciram.ing.unibo.it
[b] e-mail: andrea.mentrelli@mail.ing.unibo.it
[c] e-mail: tullio.trombetti@mail.ing.unibo.it

with few exceptions, come from idealized models of the heating process and assume that heat flows only in the direction perpendicular to the treated surface (one-dimensional heat flow), and that the workpiece is very large, compared to the spot size. As a consequence, they don't permit to evaluate the effects of the edges and corners of the workpiece, which tend to concentrate the heat flow. In addition, most of the proposed models assume that the thermal properties of the metal don't vary with temperature. In reality, heat diffusion is a three-dimensional phenomenon, the dimensions of the workpiece are often comparable with the laser spot ones and the thermal properties of the metals, especially its thermal conductivity, are not at all temperature-independent. Moreover, the majority of the developed models is devoted to study the process under quasi steady-state conditions, while a fully time-dependent model is necessary to investigate the thermal behaviour of the workpiece under realistic conditions. In addition, sometimes it is necessary to implement complex patterns of the laser spot, or to overlap hardening passes, or to take into account the presence of edges and other geometrical discontinuities of the piece [1]. As far as the authors know, no analytical expression is available for the evaluation of the effects of these events on the process result. In this framework, numerical simulation is an useful tool as it permits to reduce the idealization errors that affect the analytical expressions. It becomes also feasible to consider real workpiece geometry and complex patterns of the hardening passes. Besides that, numerical simulation may also help in optimizing the process itself. In this paper we present a numerical investigation on the effects on the thermal behaviour of the treated material of changing one or more process parameters: power of the laser beam, dimensions of the laser spot, scanning velocity and pattern are taken into account in the frame of a heating process that doesn't lead to material melting or evaporation. The temperature-dependence of the thermal properties of the treated material are carefully taken into account, as well as realistic shape and dimensions of the workpiece are examined.

2 Modelling approach

The transient three-dimensional transport equation governing the energy transfer in the workpiece excluding material melting or evaporation, written in terms of enthalpy (h) for a metal of density ρ, thermal conductivity k and constant-pressure specific heat c_p

$$\frac{\partial(\rho h)}{\partial t} = \boldsymbol{\nabla} \cdot \left(\frac{k}{c_p} \boldsymbol{\nabla} h \right) \tag{1}$$

is discretized with a finite-volume technique [11] and solved in the reference frame of the workpiece with a numerical code recently developed by the authors [12]. The solution is obtained by marching in time from a given initial uniform distribution of temperature in the workpiece (300 K). With this regard, a fully-implicit scheme is adopted. The temperature-dependence of the thermal properties of the material (stainless steel) has been suitably taken into account.

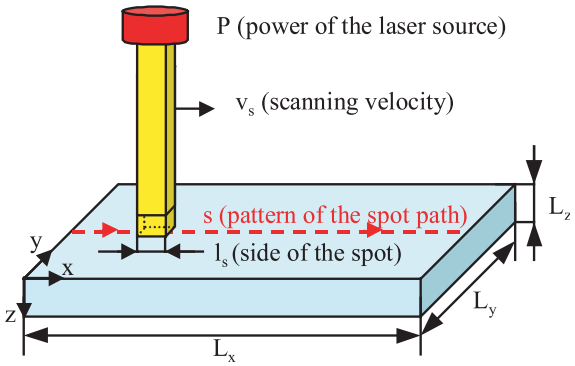

Fig. 1. Schematic of the workpiece and of the laser beam with process parameters and boundary conditions.

Since in laser surface hardening the thermal energy is generated by absorption of the laser radiation at the surface of the workpiece, no sources of thermal energy exist inside the workpiece and no source term is to be included in the governing equation: the increase of temperature in the material is exclusively due to heat conduction. Equation (1) is subject to boundary conditions that take into account the heat introduced in the piece by the laser beam, the heat dissipated at the boundary surfaces *via* convection (cooling effect of the ambient gas), and the heat radiated by the body in accordance to the Sfefan-Boltzmann's law:

$$\frac{k}{c_p} \frac{\mathrm{d}h}{\mathrm{d}n} = \alpha q - h_c \left(T - T_a \right) - \varepsilon \sigma \left(T^4 - T_a^4 \right) .$$

In this expression, the term on the left hand side represents the incoming heat flux perpendicular to the surface of the workpiece (n is the direction perpendicular to the workpiece boundary), h_c is the convection coefficient ($h_c = 2500$ W/m^{2}K); T is the surface temperature of the workpiece; T_a is the ambient temperature ($T_a = 300$ K); ϵ is the emissivity of the metal (assumed to be equal to 0.4, typical value for a polished metallic surface); σ is the Sfefan-Boltzmann constant (5.67×10^{-8} W/m^{2}K^4). The term q represents the heat flux on the surface related to the laser beam (strictly perpendicular to the boundary), which is partially absorbed by the metal, and is assumed to be zero outside the region of the surface on which impinges the laser beam (spot of the laser beam, see Fig. 1). The absorption coefficient, α, is considered to be independent from the surface temperature and equal to 70%. The spot of the laser beam is square-shaped and the heat flux is uniformly distributed over the spot ($q = P/l_s^2$, where P is the power of the laser source and l_s is the edge of the square-shaped laser spot).

3 Selected results

Time-dependent three-dimensional simulations of the laser surface heating process have been carried out by

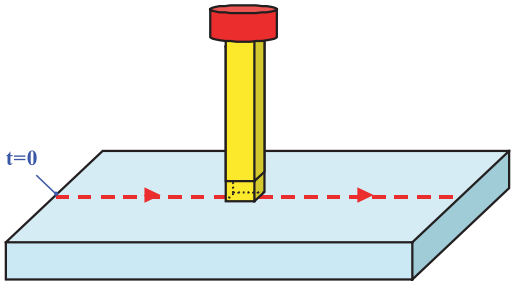

Fig. 2. Schematic of the workpiece and of the laser source moving along the x-direction with a single-pass hardening pattern.

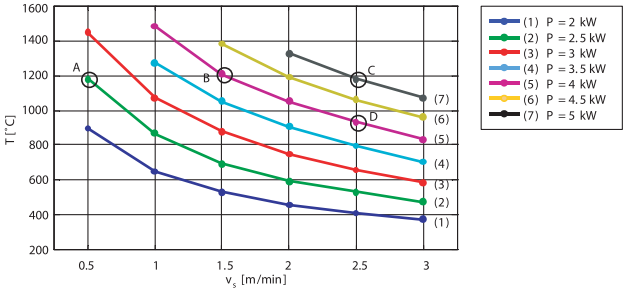

Fig. 3. Maximum temperature of the workpiece treated with a single-pass hardening pattern (see Fig. 2) for different scanning velocity (v_s) and power of the laser source (P). Common operating conditions: $L_x = 100$ mm; $L_y = 40$ mm; $L_z = 5$ mm; $l_s = 10$ mm. Temperature distributions in the workpiece for the cases indicated with letters from A to D are reported in Figures 4, 5, 6 and 7.

means of a numerical code recently developed by the authors [12]. Calculations have been carried out for various dimensions of the parallelepiped-shaped workpiece (with dimensions L_x, L_y and L_z) and of the square-shaped spot of the laser beam (with side l_s), as well as for different scanning velocities (v_s, relative workpiece — laser source velocity) and for different levels of the laser source power (P). Various patterns of the laser spot path have also been studied, including a single-pass hardening pattern (represented schematically in Fig. 2), a double-pass hardening pattern with and without an overlapping of the subsequently treated zones of the workpiece surface (represented in Fig. 11), multiple discontinuous and continuous hardening patterns (represented in Figs. 15a and 16a, respectively) and spiral hardening pattern, covered counterclockwise and clockwise (*i.e.* from the periphery to the centre of the workpiece and from the centre to the periphery, as sketched in Figs. 17a and 18a, respectively).

For the case of a single-pass hardening pattern (Fig. 2), the results of a detailed parametric study on the effects of changing the power level (P) and the scanning velocity (v_s) for fixed dimensions of the spot ($l_s = 10$ mm) and of the workpiece ($L_x = 100$ mm; $L_y = 40$ mm; $L_z = 5$ mm) are shown in Figure 3. It may be appreciated how, for a fixed power level of the laser source, an increase in the scanning velocity leads to a reduction in the maximum temperature reached in the workpiece. The same effect is associated to a reduction in the power level of the laser source for a fixed scanning velocity.

With this regard, it can be noticed that different combinations of the power level of the laser source and of the scanning velocity can lead to very similar values of the maximum temperature reached in the workpiece. For example, the three operating conditions with $P = 4$ kW and $v_s = 1.5$ m/min (case A), with $P = 2.5$ kW and $v_s = 0.5$ m/min (case B) and with $P = 5$ kW and $v_s = 2.5$ m/min (case C), all give rise to very similar values of the maximum encountered temperature, that is pretty close to 1470 K (1200 °C, for ease of comparison with most of the literature results). Nevertheless, as Figures 4a, 5a and 6a show, the time-evolution of temperature in fixed points of the workpiece (points at the centre of the horizontal planed x-y for different z coordinate, see Fig. 2) are quite different from each other. In particular, under the operating conditions of case A, both heating and quenching of the fixed points happen at lower rates than those encountered under the operating conditions of case B and case C. As a consequence, the effects of the heat treatment will be different for the three discussed situations, being the quality of the hardened zones strongly influenced by the heating and quenching rate of the thermal cycle. Ever the width and height of the hardened regions will be different in the three analyzed cases, as show the comparison between Figures 4b, 5b, 6b and Figures 4c, 5c, 6c.

Figures 6 and 7 show the effect of changing the power level of the laser source ($P = 5$ kW for case C, represented in Fig. 6 and $P = 4$ kW for case D, represented in Fig. 7), for a scanning velocity equal to 2.5 m/min and for workpiece and laser spot dimensions equal to those of the previous discussed cases. As expected, the higher the power, the higher the value of the maximum temperature reached in the workpiece. From a comparison between Figures 6c and 7c it may also be observed that a higher power level of the laser source entails a steeper temperature gradients in the surface layers.

The effects of changing the scanning velocity, keeping unchanged the power level of the laser source (equal to 4 kW), are evidenced from a comparison between Figure 5 (case B, with $v_s = 1.5$ m/min) and Figure 7 (case D, with $v_s = 2.5$ m/min). With this regard, it is interesting to note how the case with lower scanning velocity is characterized by a higher temperature of the heat affected zone but also by a lower quenching rate and by a more pronounced diffusion of the heat in the bulk of the workpiece.

Figures 8, 9 and 10 show the effects of changing the spot size ($l_s = 5$, 10 and 15 mm for Figs. 8, 9 and 10, respectively) on the temperature distribution in the workpiece for a fixed power density in the spot of the laser beam, equal to 3×10^7 W/m^2. The results are reported in the form of snapshots of the temperature distribution on the surface of the workpiece (x-y plane for $z = 0$) and on two planes perpendicular to the x- and y-axis, respectively (y-z plane for $x = 50$ mm and x-z plane for $y = 20$ mm). In all cases, the snapshots are taken when the centre of the laser spot passes through the centre of the workpiece

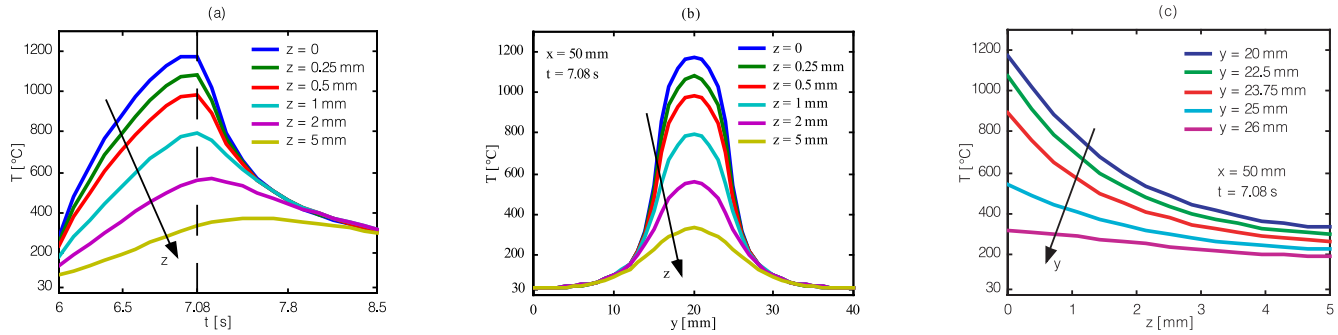

Fig. 4. (Case A) Temperature evolution on the vertical axis passing through the centre of the workpiece (a) and temperature distribution (at time $t = 7.08$ s) on a vertical plane parallel to the y-axis and passing through the centre of the workpiece (b, c). Dimensions of the workpiece: $L_x = 100$ mm; $L_y = 40$ mm; $L_z = 5$ mm. Working parameters: $P = 2.5$ kW; $v_s = 0.5$ m/min; $l_s = 10$ mm; type of pattern: single-pass hardening pattern.

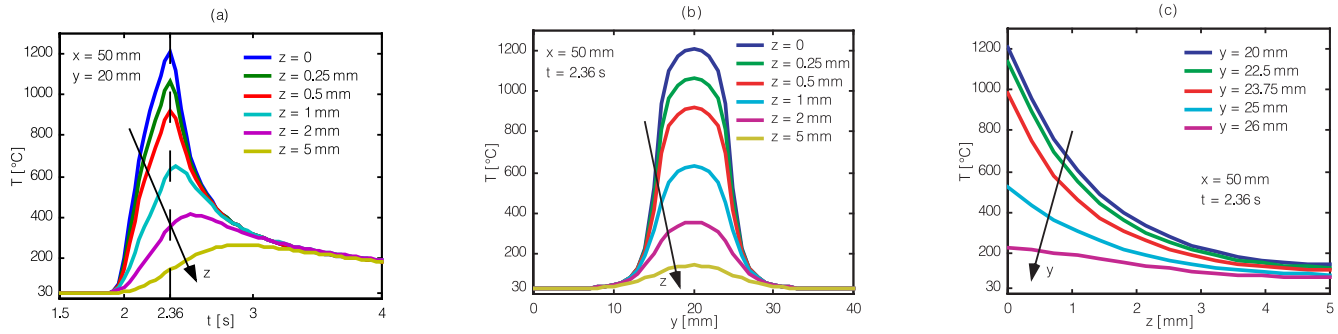

Fig. 5. (Case B) Temperature evolution on the vertical axis passing through the centre of the workpiece (a) and temperature distribution (at time $t = 2.36$ s) on a vertical plane parallel to the y-axis and passing through the centre of the workpiece (b, c). Dimensions of the workpiece: $L_x = 100$ mm; $L_y = 40$ mm; $L_z = 5$ mm. Working parameters: $P = 4$ kW; $v_s = 1.5$ m/min; $l_s = 10$ mm; type of pattern: single-pass hardening pattern.

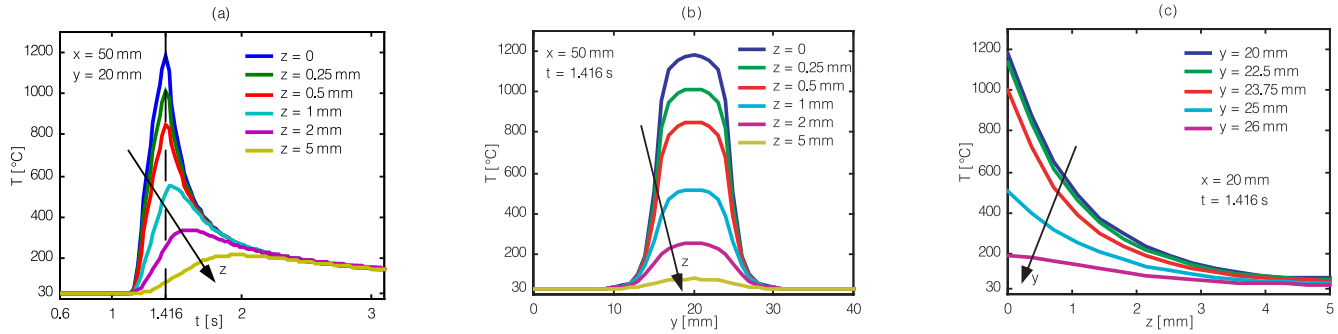

Fig. 6. (Case C) Temperature evolution on the vertical axis passing through the centre of the workpiece (a) and temperature distribution (at time $t = 1.416$ s) on a vertical plane parallel to the y-axis and passing through the centre of the workpiece (b, c). Dimensions of the workpiece: $L_x = 100$ mm; $L_y = 40$ mm; $L_z = 5$ mm. Working parameters: $P = 5$ kW; $v_s = 2.5$ m/min; $l_s = 10$ mm; type of pattern: single-pass hardening pattern.

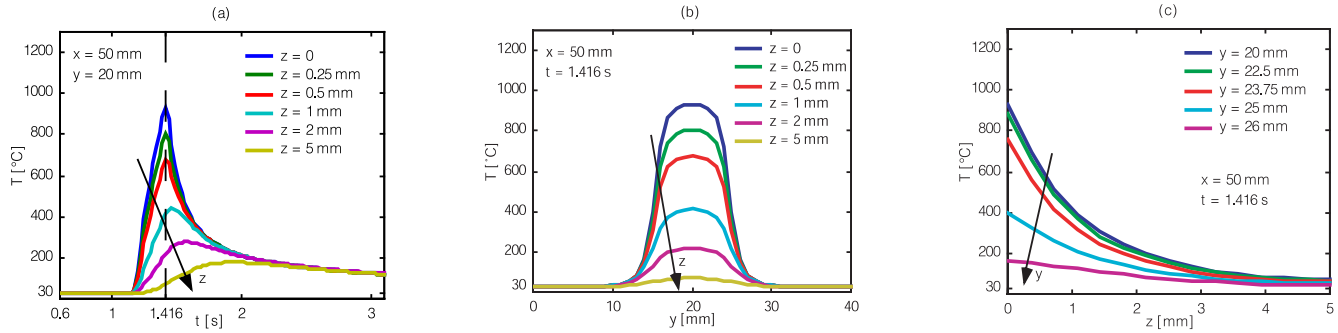

Fig. 7. (Case D) Temperature evolution on the vertical axis passing through the centre of the workpiece (a) and temperature distribution (at time $t = 1.416$ s) on a vertical plane parallel to the y-axis and passing through the centre of the workpiece (b, c). Dimensions of the workpiece: $L_x = 100$ mm; $L_y = 40$ mm; $L_z = 5$ mm. Working parameters: $P = 4$ kW; $v_s = 2.5$ m/min; $l_s = 10$ mm; type of pattern: single-pass hardening pattern.

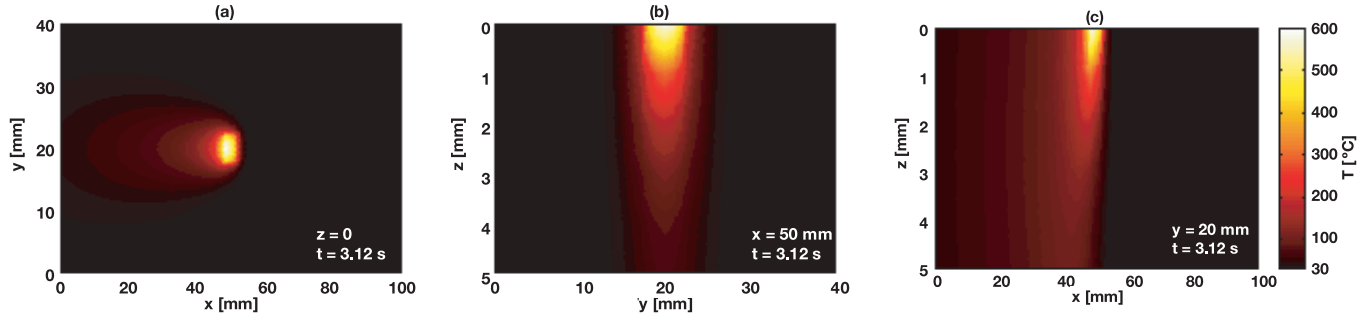

Fig. 8. Temperature distribution (at $t = 3.12$ s) on the surface of the workpiece (a) and on two planes perpendicular to the x- (b) and to the y-axis (c). Dimensions of the workpiece: $L_x = 100$ mm; $L_y = 40$ mm; $L_z = 5$ mm. Working parameters: $P = 0.75$ kW; $v_s = 1$ m/min; $l_s = 5$ mm; type of pattern: single-pass hardening pattern.

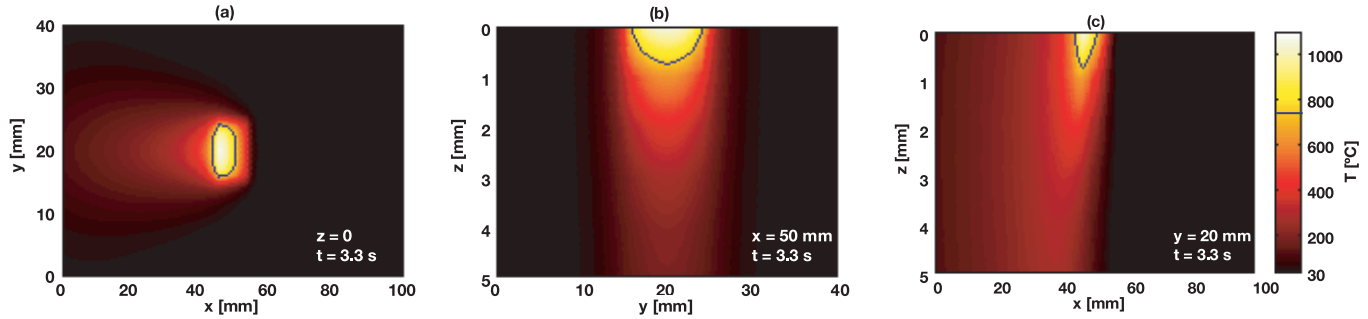

Fig. 9. Temperature distribution (at $t = 3.3$ s) on the surface of the workpiece (a) and on two planes perpendicular to the x- (b) and to the y-axis (c). Dimensions of the workpiece: $L_x = 100$ mm; $L_y = 40$ mm; $L_z = 5$ mm. Working parameters: $P = 3$ kW; $v_s = 1$ m/min; $l_s = 10$ mm; type of pattern: single-pass hardening pattern.

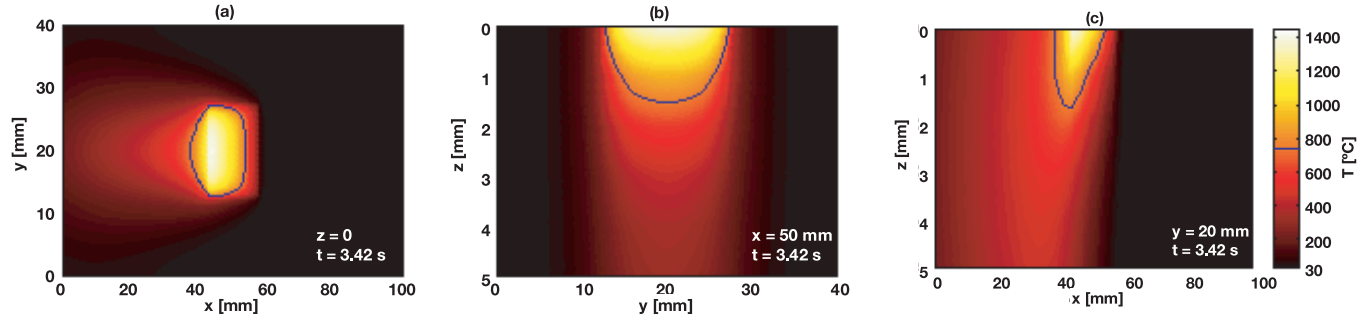

Fig. 10. Temperature distribution (at $t = 3.42$ s) on the surface of the workpiece (a) and on two planes perpendicular to the x- (b) and to the y-axis (c). Dimensions of the workpiece: $L_x = 100$ mm; $L_y = 40$ mm; $L_z = 5$ mm. Working parameters: $P = 6.75$ kW; $v_s = 1$ m/min; $l_s = 15$ mm; type of pattern: single-pass hardening pattern.

surface (*i.e.* when the coordinates of the laser spot are $x_c = 50$ mm and $y_c = 20$ mm). The scanning velocities are all equal to 1 m/min and the power level of the laser source varies from 0.75 kW when $l_s = 5$ mm (Fig. 8) to 3 kW when $l_s = 10$ mm (Fig. 9) and to 6.75 kW when $l_s = 15$ mm (Fig. 10) in order to let the power density be the same. As expected, the dimensions of the region where the temperature exceeds the austenitization temperature (assumed to be equal to 780 °C, indicated by the contour lines in the temperature maps) increase as the spot gets bigger.

The case of double-pass hardening pattern, of practical interest, has also been considered, in the situations of overlapping, non-overlapping and of a gap left between the two parallel tracks of the laser beam (see Fig. 11).

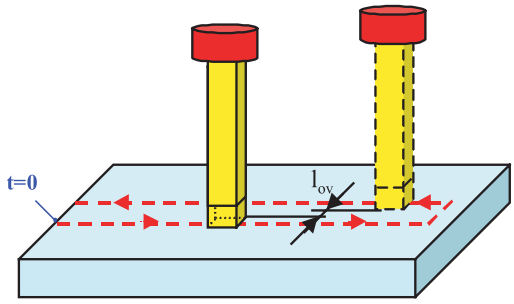

Fig. 11. Schematic of the workpiece and of the laser source moving on the workpiece surface with a double-pass hardening pattern with an overlap between the parallel tracks ($l_{ov} > 0$), with a non-overlap ($l_{ov} = 0$) or with a gap left between the two parallel tracks ($l_{ov} < 0$).

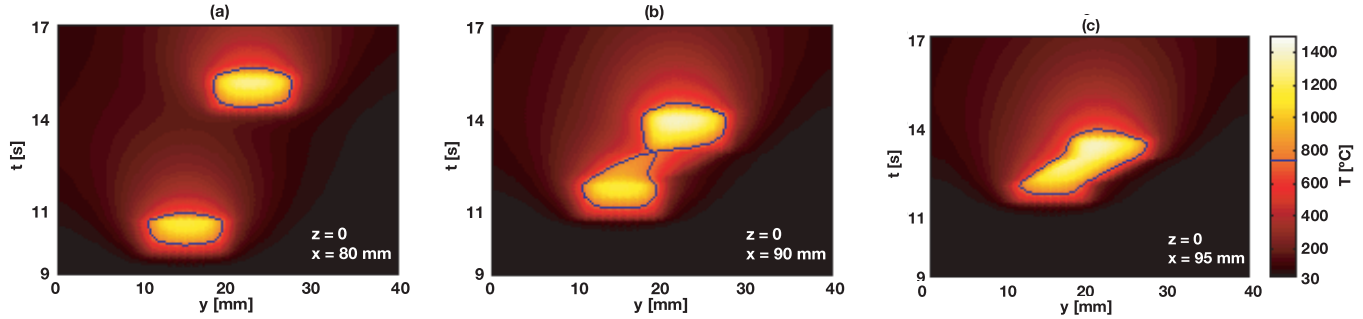

Fig. 12. Evolution of the temperature on the surface of the workpiece along the y-axis for different x positions. Dimensions of the workpiece: $L_x = 100$ mm; $L_y = 40$ mm; $L_z = 5$ mm. Working parameters: $P = 2.5$ kW; $v_s = 0.5$ m/min; $l_s = 10$ mm; type of pattern: double-pass hardening pattern with a 2 mm overlap ($l_{ov} = 2$ mm).

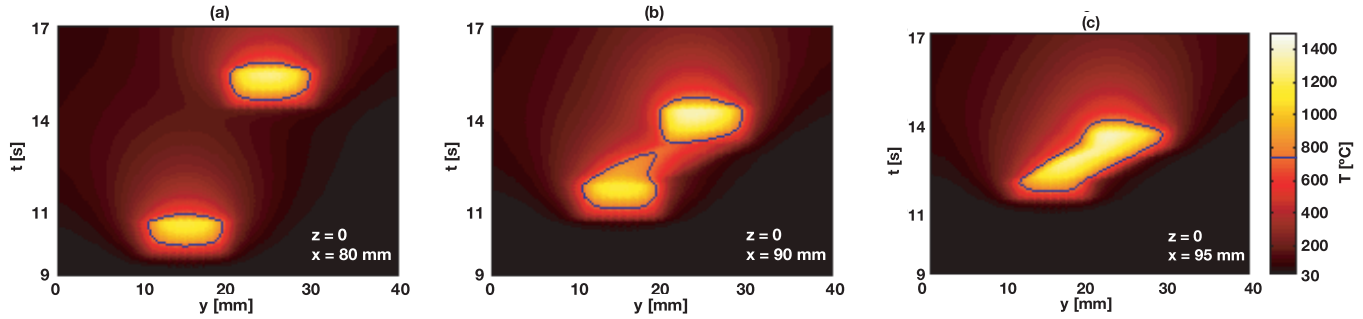

Fig. 13. Evolution of the temperature on the surface of the workpiece along the y-axis for different x positions. Dimensions of the workpiece: $L_x = 100$ mm; $L_y = 40$ mm; $L_z = 5$ mm. Working parameters: $P = 2.5$ kW; $v_s = 0.5$ m/min; $l_s = 10$ mm; type of pattern: double-pass hardening pattern with no overlap ($l_{ov} = 0$).

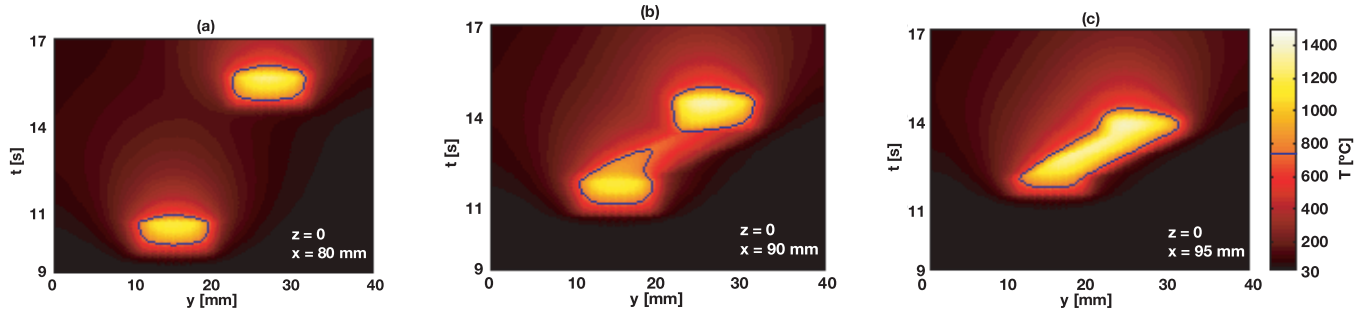

Fig. 14. Evolution of the temperature on the surface of the workpiece along the y-axis for different x positions. Dimensions of the workpiece: $L_x = 100$ mm; $L_y = 40$ mm; $L_z = 5$ mm. Working parameters: $P = 2.5$ kW; $v_s = 0.5$ m/min; $l_s = 10$ mm; type of pattern: double-pass hardening pattern with a 2 mm gap between the parallel passes ($l_{ov} = -2$ mm).

Temperature distributions in the workpiece are reported in Figures 12, 13 and 14 for cases with, respectively, an overlapping of 2 mm, a non-overlapping, and a gap of 2 mm left between the parallel tracks ($l_{ov} = 2$ mm; $l_{ov} = 0$; $l_{ov} = -2$ mm in the first, second and third case, respectively). All the simulations are relative to a case with a power level of the laser source equal to 2.5 kW, a scanning velocity of 0.5 m/min and a laser spot with a 100 mm^2 cross-section ($l_s = 10$ mm). The reported results aim at putting into evidence the time-evolution of the surface temperature along the y-direction for three different values of the x-coordinate ($x = 80$, 90 and 95 mm), in order to highlight the effects of the overlapping as the laser spot approaches the abrupt changes in directions.

Complex patterns of the laser spot path of industrial interest have also been studied: multiple-discontinuous hardening pattern (Fig. 15a), multiple-continuous pattern (Fig. 16a) and spiral pattern covered counterclockwise and clockwise, *i.e.* from the periphery to the centre of the workpiece and from the centre to the periphery, (Figs. 17a and 18a, respectively) have been studied.

For all these complex patterns, the temperature of the moving centre of the laser spot in test cases ($P = 5$ kW; $v_s = 3$ m/min; $L_x = 60$ mm; $L_y = 60$ mm; $L_z = 5$ mm; $l_s = 10$ mm) is reported in Figures 15b, 16b, 17b and 18b, showing the effects on the heating process of the different trajectories and of sharp discontinuities in the path (for the case of multiple-discontinuous hardening pattern) or

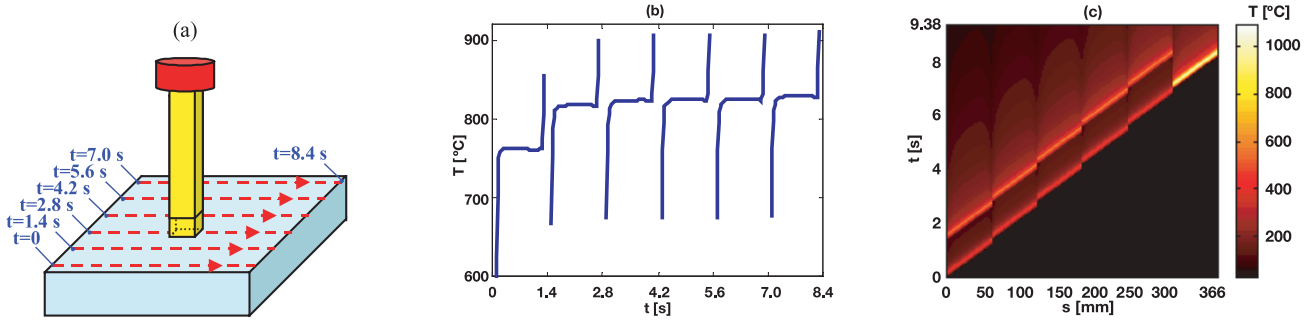

Fig. 15. Schematic of the workpiece with multiple, discontinuous hardening pattern (a); temperature evolution of the moving centre of the spot (b) and thermal history of the points laying on the workpiece surface at different positions along the path of the laser spot centre (c). Dimensions of the workpiece: $L_x = 60$ mm; $L_y = 60$ mm; $L_z = 5$ mm. Working parameters: $P = 5$ kW; $v_s = 3$ m/min; $l_s = 10$ mm.

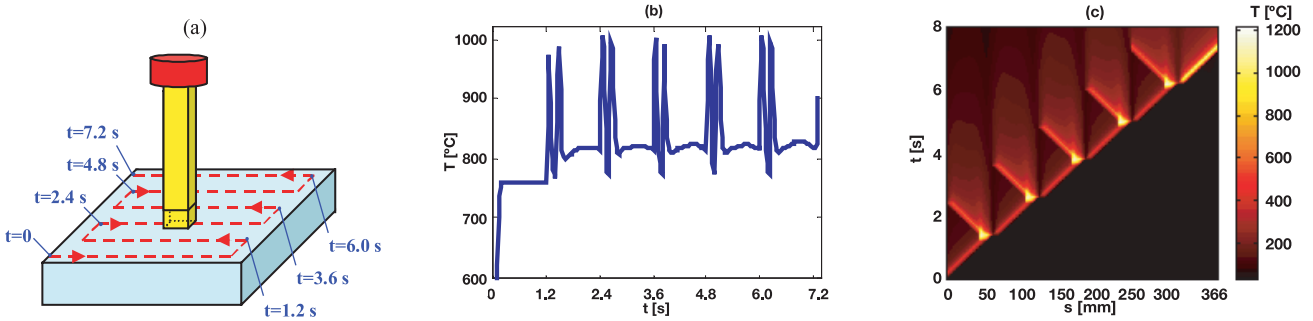

Fig. 16. Schematic of the workpiece with multiple, continuous hardening pattern (a) and temperature evolution of the moving centre of the spot (b) and thermal history of the points laying on the workpiece surface at different positions along the path of the laser spot centre (c). Dimensions of the workpiece: $L_x = 60$ mm; $L_y = 60$ mm; $L_z = 5$ mm. Working parameters: $P = 5$ kW; $v_s = 3$ m/min; $l_s = 10$ mm.

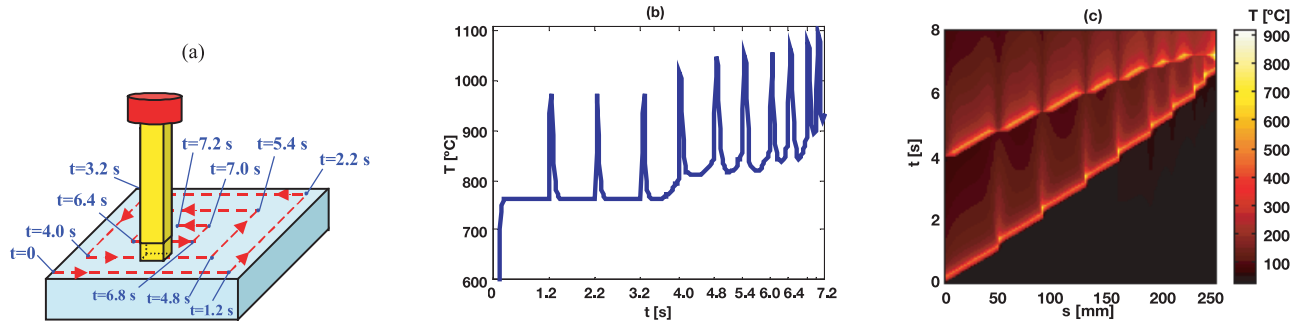

Fig. 17. Schematic of the workpiece with spiral hardening pattern from the periphery to the centre (a) and temperature evolution of the moving centre of the spot (b) and thermal history of the points laying on the workpiece surface at different positions along the path of the laser spot centre (c). Dimensions of the workpiece: $L_x = 60$ mm; $L_y = 60$ mm; $L_z = 5$ mm. Working parameters: $P = 5$ kW; $v_s = 3$ m/min; $l_s = 10$ mm.

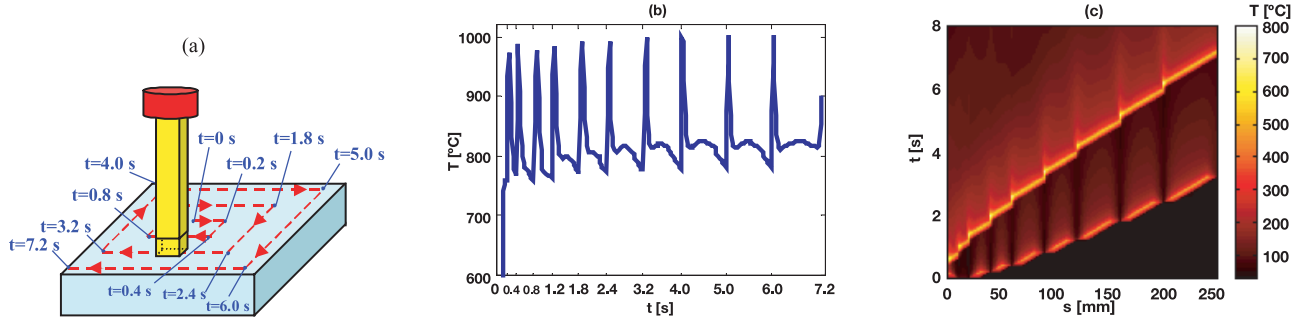

Fig. 18. Schematic of the workpiece with spiral hardening pattern from the centre to the periphery (a) and temperature evolution of the moving centre of the spot (b) and thermal history of the points laying on the workpiece surface at different positions along the path of the laser spot centre (c). Dimensions of the workpiece: $L_x = 60$ mm; $L_y = 60$ mm; $L_z = 5$ mm. Working parameters: $P = 5$ kW; $v_s = 3$ m/min; $l_s = 10$ mm.

abrupt changes in direction of the laser spot (for the case of multiple-continuous and spiral hardening patterns).

Figures 15c, 16c, 17c, 18c show the time-evolution of the temperature along the curvilinear coordinate s of the moving centre of the laser spot. From these results, information concerning the changing in time of the temperature of the points laying on the workpiece surface along the path of the centre of the laser spot may be extracted. This kind of representation of the results permits a visualization of the temperature history of the points that lay on the path of the moving laser spot centre.

In all cases, it is appreciable how an abrupt change in direction of the laser spot, or a discontinuity in its path, turns into a peak in the local temperature in the proximity of the singularity. This is one of the major drawbacks of complex patterns, as it may lead to a loss of uniformity in the thermal treatment.

The presented results show how the proposed model can be usefully employed in the prediction of the time-evolution of temperature distribution which arises in a parallelepiped-shaped workpiece as a consequence of the laser-workpiece interaction, in absence of material melting or evaporation, under operating conditions typically encountered in industrial applications of the laser hardening process. As a next step, experiments will be performed in order to compare experimental data concerning the temperature reached in the workpiece and the results obtained by means of the simulation tools developed by the authors. With this regard, a 3 kW CO_2 laser source will be employed. Experimental work will also include hardness tests as well as internal stress measurements conducted using mechanical relaxation methods.

The authors would like to thank Maichi Cantello and Federico Giachino at RTM in Vico Canavese (Italy) for the useful suggestions and discussions concerning laser surface hardening process and operating conditions. This work was performed with partial financial support from the University of Bologna Goal-Oriented project 2001-2003 and ex-60% 2001-2002 projects, from the Italian Ministry of Education, University and Scientific Research (MIUR) national project COFIN 2002 and National Group for Mathematical Physics (GNFM) of the Italian Institute of High Mathematics.

References

1. O.A. Sandven, *Laser Surface Hardening, Metal Handbook* (ASM International), pp. 286-296
2. W.M. Steen, *Laser Material Processing* (Springer Verlag, London, 1991)
3. J. Mazumder, W.M. Steen, J. Appl. Phys. **51**(2), 941 (1980)
4. S. Kou, D.K. Sun, Y.P. Le, Metall. Trans. A **14**, 643 (1983)
5. G. Ricciardi, M. Cantello, G.F. Micheletti, *Technological applications of the laser beam in heat treatments*, Ann. ICRP (International Institution for Production Engineering Research), STC E, pp. 125-130 (1982)
6. J. Mazumder, P.S. Mohanty, A. Kar, Int. J. Mat. Prod. Technol. **11**, 193 (1996)
7. R. Komanduri, Z.B. Hou, Int. J. Heat Mass Transfer **44**, 2845 (2001)
8. A. Yánez, J.C. Álvarez, A.J. López, G. Nicolás, J.A. Pérez, A. Ramil, E. Saavedra, Appl. Surf. Sci. **186**, 611 (2002)
9. R. Brockmann, K. Dickmann, P. Geshev, K.-J. Matthes, Int. J. Heat Mass Transfer **46**, 717 (2003)
10. A. Kar, J. Mazumder, J. Appl. Phys. **65**, 2923 (1989)
11. S. Patankar, *Numerical heat transfer and fluid flow* (McGraw-Hill, New York, 1980)
12. A. Mentrelli, V. Colombo, T. Trombetti, Time-dependent 3-D modelling of laser & plasma surface heating for the hardening of metallic materials, *Proceedings of the 16th International Symposium on Plasma Chemistry (ISPC-16)*, Taormina, Italy, 23-27 June 2003 (paper ISPC-638)